Virus Research 259 (2019) 97–107

Contents lists available at ScienceDirect

Virus Research

journal homepage: www.elsevier.com/locate/virusres

Characterization of maize translational responses to sugarcane mosaic virus infection

Tengzhi Xu[a,1], Lei Lei[a,c,1], Junpeng Shi[b], Xin Wang[b], Jian Chen[b], Mingshuo Xue[a], Silong Sun[b], Binhui Zhan[a], Zihao Xia[a], Na Jiang[a], Tao Zhou[a], Jinsheng Lai[b], Zaifeng Fan[a,*]

[a] State Key Laboratory of Agrobiotechnology and Key Laboratory of Pest Monitoring and Green Management-MOA, China Agricultural University, Beijing 100193, PR China

[b] State Key Laboratory of Agrobiotechnology and National Maize Improvement Center, Department of Plant Genetics and Breeding, China Agricultural University, Beijing 100193, PR China

[c] Guizhou Rapeseed Institute, Guizhou Academy of Agricultural Sciences, Guiyang 550008, PR China

ARTICLE INFO

Keywords:
Sugarcane mosaic virus
Ribosome profiling
Translational response
Photosynthesis
Zea mays

ABSTRACT

Sugarcane mosaic virus (SCMV) frequently causes dramatic losses in maize production as the main pathogen of maize dwarf mosaic disease. It is important to understand the translational responses in maize to SCMV infection since viruses have to recruit host translation apparatus to express their proteins. However, due to technical limitations, research on virus translation lags far behind that on transcription. Here, we studied the relationship between systemic symptom expression and virus accumulation and found that both SCMV RNA and proteins accumulated rapidly during the systemic infection process in which varying degrees of chlorosis to mosaic symptoms developed on non-inoculated leaves. In addition, we applied ribosome profiling, which couples polysomal mRNA isolation with high-throughput sequencing, on the symptomatic leaves infected with SCMV to unravel the translational responses of maize to viral infection on a genome-wide scale. The results showed that only the genomic positive-stranded RNA of SCMV was involved in translation, and SCMV only occupied a small amount of translational resources of host plant at the early stage of infection. Further analyses on a global gene expression and gene ontology (GO) enrichment revealed that photosynthesis and metabolism were dramatically repressed at both transcriptional and translational levels. Altogether, our results laid a foundation for dissecting the molecular mechanism of plant translational responses to viral infection.

1. Introduction

Sugarcane mosaic virus (SCMV) is one of the most hazardous plant viral pathogens prevalent in China as the main causal agent of maize dwarf mosaic disease. SCMV infects maize (*Zea mays* L.), sugarcane (*Saccharum sinensis*), sorghum (*Sorghum vulgare*) and many other poaceous species and usually causes significant losses in grain yields (Shukla et al., 1989). For maize, chlorotic symptoms of SCMV infection first occur at the base parts of the leaf and extend to the whole leaf into stripe mosaic pattern. SCMV is a member of the genus *Potyvirus* in the family *Potyviridae*, which is one of the largest plant virus families (Le et al., 1999; Riechmann et al., 1992; Gibbs and Ohshima, 2010). SCMV genome consists of a linear positive-sense and single-stranded RNA of 9595 or 9596 nucleotides (nt). The 5′ terminus of genomic RNA covalently bonds to a viral protein VPg with a tyrosine residue while the 3′ end of genomic RNA contains a polyadenylated tail. As for picornaviruses, VPg is removed from the polysome-associated viral RNAs prior translation (Nomoto et al., 1977), however, whether or not similar event happens with potyviral RNAs remains an open question. Although potyvirus VPg recruits host translation factors eIF4E/eIFiso4E (Charron et al., 2008; Léonard et al., 2004), no direct evidence yet indicates that VPg participates in translation. Cap-independent translation is likely mediated by the 5′-UTR by analogy with analyses conducted with related viruses (Kneller et al., 2006). SCMV contains a large open reading frame (ORF) which encodes a polyprotein of *ca.* 344 kD. The polyprotein is autocatalytically cleaved into ten separate proteins namely P1, HC-Pro, P3, 6K1, CI, 6K2, VPg, NIa-Pro, NIb, and CP to execute corresponding functions (Urcuqui-Inchima et al., 2001; Merits et al., 2002). A short ORF, *pipo*, generated through a +2 transcriptional slippage within the P3 cistron, encodes a polypeptide fused to the N-

* Corresponding author.
E-mail address: fanzf@cau.edu.cn (Z. Fan).
[1] These authors contributed equally to this work.

https://doi.org/10.1016/j.virusres.2018.10.013
Received 8 July 2018; Received in revised form 14 October 2018; Accepted 18 October 2018
Available online 21 October 2018

terminal portion of P3 as P3N-PIPO, which is now considered as a common potyviral product (Chung et al., 2008; Olspert et al., 2015; Rodamilans et al., 2015). As is the case for P3N-PIPO, P3N-ALT, which is another transcriptional slippage product in the +1 reading frame of P3 cistron was recently identified in a potyvirus clover yellow vein virus (ClYVV) (Hagiwara-Komoda et al., 2016). Another short ORF termed *pispo* was reported to overlap the P1 cistron with an equivalent polymerase slippage event as PIPO in a few members of the *Potyvirus* genus (Rodamilans et al., 2015; Mingot et al., 2016; Olspert et al., 2016; Untiveros et al., 2016).

As an early and critical step of plant virus infection cycle, translation is a strictly regulated process that includes several phases, namely initiation, elongation, termination and ribosome recycling. Although plant viruses encode a certain number of requisite proteins, their coding capacity is limited due to their relatively small genome. As obligate intracellular parasites, viruses gain access to the protein synthesis machinery by partially hijacking the host cellular pathways and manipulating cellular components for translation of their mRNAs (Gebauer and Hentze, 2004; Sanfaçon, 2015). However, viral occupation of host translational resources as well as the translational responses of hosts to viral infection have rarely been studied.

Combined with bioinformatic analysis, high-throughput sequencing has been used in novel virus identification (Kehoe et al., 2014), virus detection and diagnosis (Wylie et al., 2012; Nagano et al., 2015), population variation and evolution analysis (Kutnjak et al., 2015) and small RNA analysis (Xia et al., 2014; Herranz et al., 2015), *etc.* In recent years, a promising powerful technique called ribosome profiling (Ribo-Seq) based on ribosome footprints and high throughput sequencing was reported first on budding yeast and then on plant, which provides snapshots on genome-wide translation profiles (Ingolia et al., 2009; Liu et al., 2013; Juntawong et al., 2014; Lei et al., 2015). General workflow to perform ribosome profiling analysis includes the ribosome-protected mRNA fragments (RPFs) isolation from total mRNAs subjected to RNase digestion and the sequencing library construction. Through sequencing RPFs, ribosome profiling enables us to access the positions and average number of ribosomes on a given transcript at a subcodon resolution (Ingolia et al., 2011). Ribosome profiling has been widely applied to the understanding of complex translational mechanisms (Ingolia et al., 2011; Gerashchenko et al., 2012; Michel et al., 2012; Chew et al., 2013; Dunn et al., 2013; Guttman et al., 2013; Shalgi et al., 2013), identifying coding sequence regions and quantifying the gene expression at translational level (Juntawong et al., 2014; Lei et al., 2015). Ribosome profiling has been used to define human cytomegalovirus (HCMV) translation products to reveal its coding potential (Stern-Ginossar et al., 2012). As a result, 751 ORFs were identified, including 245 ORFs which potentially encode polypeptides consisted of less than 20 amino acids and were hardly detected by mass spectroscopy, demonstrating that the potential role of ribosome profiling in deciphering viral complexity.

Our previous work has unraveled the ribosome profiling in maize and the translational responses to drought stress (Lei et al., 2015). In this research, we characterize the symptom development with the infection of SCMV in maize and have performed both ribosome profiling and RNA-seq on the leaves during early infection stage. To our knowledge, this is the first report on using ribosome profiling to understand the responses of a host plant to early viral infection.

2. Materials and methods

2.1. Plant materials preparation

Maize inbred line B73 was used in this study. Seeds were surface-sterilized by immersion in an aqueous solution of 0.5% sodium hypochlorite for 30 min and then repeatedly washed to remove residues. Seeds were germinated in the dark for 2–3 days at 25 °C between layers of moist paper towels to allow the uniform elongation of the mesocotyl. Seedlings uniformly germinated were then transplanted into pots containing soil mixture (vermiculite: soddy soil = 1:1, v/v) and were cultivated in a greenhouse under a regime of 16 h light (24 °C) and 8 h dark (20 °C). The first true leaves of the maize seedlings at two- to three-leaf-stage (6–7 days after sowing) were mechanically inoculated with SCMV-BJ isolate (accession number AY042184) (Fan et al., 2003) or inoculation buffer (as mock-inoculated control). The first systemically infected leaves were harvested at different days post inoculation, then quickly frozen in liquid nitrogen and stored in a −80 °C freezer.

2.2. qRT-PCR

qRT-PCR analysis was conducted to measure SCMV accumulation, validate the RNA-seq and Ribo-Seq results. Two biological samples were used respectively: one was the ground leaves and the other was the isolated polysomes. Total RNAs from the samples were extracted using TRIzol reagent (Invitrogen) and treated with RNase-free DNase I (TaKaRa) to eliminate genomic DNA. An aliquot of 40 μg of total RNA was converted into cDNA (RT product) with M-MLV reverse transcriptase (Promega) using oligo (dT) as primer for SCMV accumulation analysis or a mixture of oligo (dT) and random primers for RNA-seq and Ribo-seq results validation according to the manufacturer's instructions, yielding 20 μL of cDNA solutions. The cDNA was diluted 10-fold as the template for the qRT-PCR. Each qPCR reaction mixture consisted of 2 μL of the diluted cDNA, 10 μL of SYBR® Premix Ex Taq™II (TaKaRa), 0.4 μL of ROX reference Dye II, 0.4 μL of forward primer (10 μM) and 0.4 μL of reverse primer (10 μM) in a total volume of 20 μL. Reactions were performed in triplicate to ensure consistent technical replication and run in 96-well plates under the following thermal cycling conditions: 95 °C for 30 s, and 40 cycles of 95 °C for 5 s and 58 °C for 34 s. Melting curves (58 °C to 95 °C) were derived for each reaction to ensure a single product. The real-time PCR system ABI 7500 (Applied Biosystems) was used.

The sequences of primer pair for SCMV genomic RNA amplification were 5′-ATTTGGTTGCGTCAGCGGTT-3′/5′-ACACCACCAGGACGAGAATGC-3′ (4090–4217 nt). Primer pairs for the RNA-seq and Ribo-seq data validation were designed using the software package Primer Premier 6.0 and the sequences were listed in Table S11. Gene expression levels were normalized to maize *ubiquitin* gene (U29159). Gene relative expression levels was estimated by corresponding gene in mock samples by using the comparative $\Delta\Delta C_T$ method with the primer pair sequences of 5′- GGAAAAACCATAACCCTGGA-3′/5′-ATATGGAGAGAGGGCACCAG-3′ (3737–4001 nt).

2.3. Semi-quantitative RT-PCR analysis

Total RNA isolation and cDNA synthesis were performed as described above, except each RNA sample was quantified as 0.5 μg/μL before reverse transcription. SCMV RNA is determined by semi-quantitative RT-PCR with primers of 5′-ATTTGGTTGCGTCAGCGGTT-3′/5′-ACACCACCAGGACGAGAATGC-3′ (4090–4217 nt). *Ubiquitin* gene was quantified as the internal control with the primers of 5′- GGAAAAACCATAACCCTGGA-3′/5′-ATATGGAGAGAGGGCACCAG-3′. PCR amplification was performed at 95 °C for 5 min, following 30 cycles of 95 °C for 30 s, 60 °C for 30 s and 72 °C for 30 s. Load 5 μL of amplification product in 1.5% agarose gel to visualize.

2.4. Immunoblotting measurement of SCMV CP levels

Total proteins were extracted with the lysis buffer [10 mM HEPES (pH 7.5), 100 mM NaCl, 1 mM glycerol and 0.5% TritonX-100]. Protein concentration was determined using Bradford protein assay according to the instruction (Bio-Rad). Total of 30 μg protein was loaded onto 10% sodium dodecyl sulfate-polyacrylamide gel electrophoresis (SDS-PAGE) for 2 h and then transferred to a PVDF membrane (Bio-Rad) by an electrophoretic transfer system. The blots were blocked for 30 min in 5% non-fat milk in PBST (PBS containing 0.05% Tween 20), and

subsequently incubated with anti-SCMV CP antibody (diluted 1: 5000) for 1 h at room temperature. Then the blots were washed three times with TBST and probed with horseradish peroxidase (HRP)-conjugated secondary antibody. After washing three times with TBST, the probed proteins were visualized with ECL Western blotting detection system (Bio-Rad) according to the user manual.

2.5. RNA-seq

Systemically infected leaves with symptoms were collected as SCMV-infected samples. Mock-inoculated leaves were harvested as a control. Total RNA was extracted using the TRIzol reagent (Invitrogen). Sequence libraries were prepared following the manufacturer's instruction of the Illumina Standard mRNA-seq library preparation kit (Illumina, http://www.illumina.com/). Libraries were sequenced by paired-end 2*101 nt (both ends with 101 nucleotides long) on an Illumina HiSeq 2500 platform.

2.6. Ribosome profiling

We took systemically infected leaves with stage 3 phenotype at 7 DPI as SCMV-infected samples for ribosome profiling. Mock-inoculated leaves at 7 DPI were collected as control. Ribosome profiling was performed as reported previously (Lei et al., 2015). Briefly, precooled polysome extraction buffer (30 mL) [200 mM Tris-Cl (pH 9.0), 200 mM KCl, 25 mM EGTA, 35 mM $MgCl_2$, 0.2% Brj-35, 0.2% TritonX-100, 0.2% Igepal CA630, 0.2% polyoxyethylene 10 tridecyl ether, 5 mM DTT, 100 mg mL^{-1} cycloheximide, 100 mg mL^{-1} chloramphenicol, and a complete proteinase inhibitor cocktail] was added to a 15 mL fine powdered leaf tissue aliquot, and the tube was vortexed. The homogenate was filtered through a double layer of miracloths and further clarified by centrifugation at 10,000 g for 15 min at 4 °C. The crude centrifugal supernatant was filtered and centrifuged repeatedly, then loaded onto the top of a 1.7 M sucrose solution and centrifuged at 50,000 rpm for 3 h at 4 °C (Beckman, Ti70 rotor). The pellet was resuspended in 600 μL of RP buffer [20 mM Tris-Cl (pH 8.0), 150 mM NaCl, 5 mM $MgCl_2$, 1 mM DTT and 100 μg mL^{-1} cycloheximide, 100 μg mL^{-1} chloramphenicol] and incubated on ice for 30 min.

About 600 μL of the resultant ribosome supernatant was subjected to 1 h digestion at 20 °C with 15 μL RNase I (Invitrogen) and then stopped by adding 20 μL RNase Inhibitor (Invitrogen). Finally, monosomes were fractionated by centrifugation at 50,000 rpm (Beckman, SW55.1 rotor) for 1.5 h at 4 °C over a 4.5 mL sucrose density gradient (15–60% w/v). RPFs were extracted with miRNeasy RNA isolation kit (Qiagen). Small RNA fragments of 26–34 nt in length were collected by gel extraction with universal miRNA linker (BioLabs) added for ligation. The ligation products were then subjected to reverse transcription and circularization. rRNAs were removed as previously reported (Juntawong et al., 2014) with eight synthesized rRNA probes according to the reported data in maize (Table S3) (Lei et al., 2015). Sequence libraries were ultimately developed with the ligation products which were purified and enriched using the QIAquick PCR Purification Kit. Ribosome profiling libraries were sequenced using single-end 50 nt reads on an Illumina sequencing (Hiseq 2500) platform.

2.7. Polysome levels calculation

Optical density (OD) of the samples was measured with an EM-1 Econo UV Monitor (Bio-Rad) and Model 251 Gradient Profiler (GP) (Biocomp Instruments, Fredericton, NB, Canada) reading absorbance throughout the sucrose gradient at 254 nm. The area under the polysome profile with the gradient baseline OD (absorbance of a gradient loaded with extraction buffer) subtracted was calculated to determine the polysome levels. Monosomes include 80S ribosome and one ribosome per transcript, while polysomes were those with two or more ribosomes per transcript. The levels were determined by calculating their corresponding peak areas and shown as a percentage of the total area under the profile. The lower boundary was the 40S subunit peak and the upper boundary was the end of the largest polysome profile.

2.8. Processing of ribosome profiling raw data

Raw sequence reads in FASTQ format were first trimmed from the adapter sequence 5′-CTGTAGGCAC-3′ with the Fastx_Clipper command of FASTX-Toolkit tools. Then, the reads were mapped to the ribosomal DNA reference sequences downloaded from NCBI to filter the aligned rRNA reads with Bowtie (v0.12.9) (Langmead et al., 2009). The remaining reads (clean data) were mapped to the B73 genome (RefGen_v2) using Tophat (v2.1.0) with the default value (Trapnell et al., 2009; Lei et al., 2015).

2.9. 3-nt periodicity analysis

To accurately map each position, the 5′-end of each read was used. According to the number of corresponding site, the reads were also plotted to analyze 3-nt periodicity. Based on the formula: $i = 4 \times \text{read number}_i$ /(read number_{i-2} + read number_{i-1} + read number_{i+1} + read number_{i+2}), relative phase of position was calculated. Unique mapped reads were extracted according to different read lengths (27–34 nt). Then, the position of 5′-end of each read located relative to CDS (coding sequence) start sites and stop codon sites was used to construct density maps.

2.10. Identification of differentially expressed genes and GO analysis

Cuffdiff (v2.2.1) was employed to analyze differentially expressed genes. Expressional abundance of each gene, measured by FPKM value, was calculated by Cufflinks (v2.2.1) with reads (Trapnell et al., 2009). Only reads mapped to the maize B73 genome (RefGen_v2) and located in CDSs were calculated. Differential expression of genes was modulated significant if the false discovery rate (FDR) was calculated to the correct P-value (controlling the expected FDR to no more than 0.01) and $\log_2$ (fold change of FPKM) > = 1. Identification (ID) of these genes were subjected to singular enrichment analysis (SEA) in AgriGO (http://bioinfo.cau.edu.cn/agriGO/) with *Zea mays* ssp V5a chosen as the supported species, all IDs were allowed to be analyzed in this type mode. The up- and down-regulated genes that fell into three categories including biological process, cellular component and molecular function. Significance of enrichment is indicated by a p-value of < 0.01.

2.11. De novo SCMV genome assembly

De novo SCMV genome assembly of the SCMV-mapped reads was performed using SOAP denovo software with parameters: '-K 19 –R' (v1.05, http://soap.genomics.org.cn). The minimum of 300 nt assembled fragments in length were allowed and further joined into scaffolds. Mapping results were visualized using the Integrative Genomics Viewer (IGV) software, which is available at http://www.broadinstitute.org/igv/.

3. Results

3.1. Characterization of the viral accumulation in the first systemically infected leaves

To characterize the viral accumulation upon SCMV infection, we first investigated the relationship between systemic symptom development and viral accumulation upon SCMV infection. Groups of more than 100 maize seedlings (inbred line B73) were mechanically inoculated with SCMV in each independent experiment. For the duration of each experiment, all seedlings were placed under the same culture conditions. The severity of disease symptoms and the percentage of

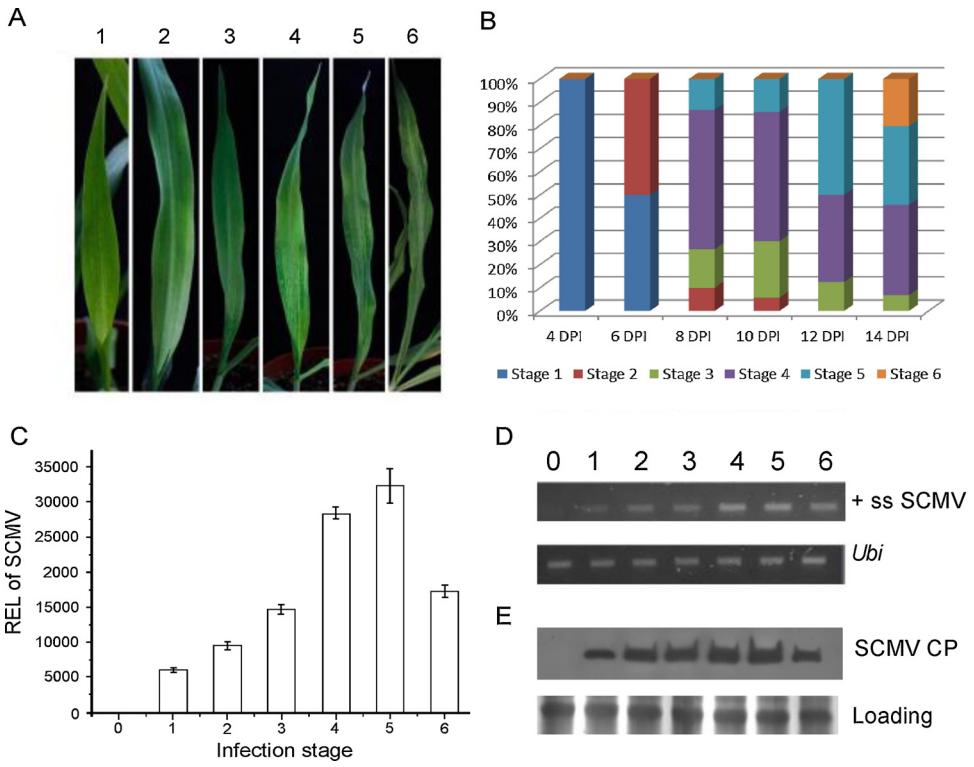

Fig. 1. Symptoms development and SCMV accumulation in first systemically infected maize leaves.
(A) Mosaic symptom development and the corresponding symptoms developmental stages. Stages were numbered from 0 to 6. (B) Statistics on the number of SCMV infected maize seedlings with symptom over time. (C) Relative expression levels of SCMV RNA of different infection stages. (D) Semi-quantitative RT-PCR analysis of SCMV RNA of different infection stages. Ubi is used as an internal control. (E) Western blotting analysis of SCMV CP accumulation of different infection stages. The numbers represent different infection stages, except for zero, which refers to samples of mock inoculation.

seedlings with the first systemically infected leaves exhibiting symptoms were recorded.

We divided the infection process into six stages based on the severity of the development of mosaic symptom on the first systemically infected leaves as shown in Fig. 1A. At 4 days post inoculation (DPI), 35% of the first systemically infected leaves began to show mild mottling and chlorosis, and these symptoms developmental period was set arbitrarily as stage 1 (Fig. 1A and B and Table S1). At 6 DPI, half of the seedlings had developed the symptoms with more severe chlorosis at the base of first systemically infected leaves (stage 2) (Fig. 1A and B and Table S1). At 8 DPI, 8.3% of diseased leaves turned pale yellow from chlorosis at the basal part of leaves (stage 3), while some dark green islands gradually appeared on the chlorotic leaves (stage 4) which account for approximately 30% of diseased leaves in this period (Fig. 1A and B and Table S1). Two days later, the mosaic symptom on 8.3% of the diseased plants covered over 1/3 areas of the leaf (stage 5) (Fig. 1A and B and Table S1). Besides, 14.1% and 32.5% of diseased leaves showed the 3rd and 4th stage symptom, respectively. The disease incidence of this period reached the maximum at 58.3% (Fig. 1B and Table S1). At 12 DPI, the percentages of diseased plants in stages 4 and 5 were increased to 20.7% and 27.6%, respectively (Fig. 1B and Table S1). At 12 DPI, about 10.9% of seedlings were of stage 6, with the mosaic symptom expanding to more than half of the first systemically infected leaves which began to show yellowing (Fig. 1A and B and Table S1), also accompanied by the full expansion of the second systemically infected leaves with mosaic symptoms evenly distributed. Stage 0 represents a group of dead or uninfected seedlings.

In addition, to quantify the corresponding kinetics of virus RNA and protein synthesis during the disease symptom development, the first systemically infected leaves of each stage at a single infection timepoint were collected. Quantitative real-time RT-PCR and semi-quantitative RT-PCR analyses for SCMV RNA showed a persistent transcripts increase at the first five stages while slightly reduced at the last stage, which may be due to leaf senescence (Fig. 1C and D). Immunoblot results indicated that the viral coat protein (CP) accumulation followed the similar pattern as viral RNA (Fig. 1E). These results indicate that gradual symptoms increase accompany with the gradual accumulation of virus, and demonstrate the rationality of the stages division.

Quantitative real-time RT-PCR results showed that SCMV increased sharply from stage 3 and stage 4 (Fig. 1C). It indicated that virus proliferate actively in maize between this two stages. To systematically explore the impact of SCMV infection on maize at transcriptional and translational levels, we used the first systemically infected leaves of stage 3 at 7 DPI for further research.

3.2. RNA sequencing and ribosome profiling analysis of SCMV-infected maize seedlings

Next, we performed parallel RNA-seq and Ribo-seq analysis on both SCMV-infected and mock-inoculated maize seedlings. Two independent biological replicates were prepared with the first systemically infected leaves at stage 3 (Table S2). Mock-inoculated controls under the same growth period and conditions were also analyzed with two replicates (Table S2). Pearson correlation coefficient demonstrated a good reproducibility among these replicates (Figure S1). After rRNA reads were filtered out of raw reads, ribosome protected reads were mapped against the maize B73 reference genome (RefGen_v2) and SCMV reference genome (GenBank accession number: AY042184) (Fan et al., 2003). As a result, ~16% and ~24% reads were mapped on B73 genome of SCMV-infected sample and mock-inoculated control, respectively, which were higher than 12% as previously reported in maize (Lei et al., 2015). The increased proportion may be due to rRNA removal in library construction (Juntawong et al., 2014) with eight synthesized rRNA probes according to the reported data in maize (Methods and Table S3). The average size of RPFs isolated from leaf tissues was around 32 nt in length among those samples (Fig. 2A). Translating ribosome steps forward three nucleotides one time and ribosome profiling can accurately capture the triplet periodicity during translation (Ingolia et al., 2009; Chew et al., 2013; Lei et al., 2015). Using the 5′ end of each read as a coordinate, we calculated the number of uniquely mapped reads located at each nucleotide after the start codon and obtained a strong three-nucleotide periodicity in both SCMV-infected and mock-inoculated maize sample data (Fig. 2B). These results showed that RNA sequencing and ribosome profiling had been

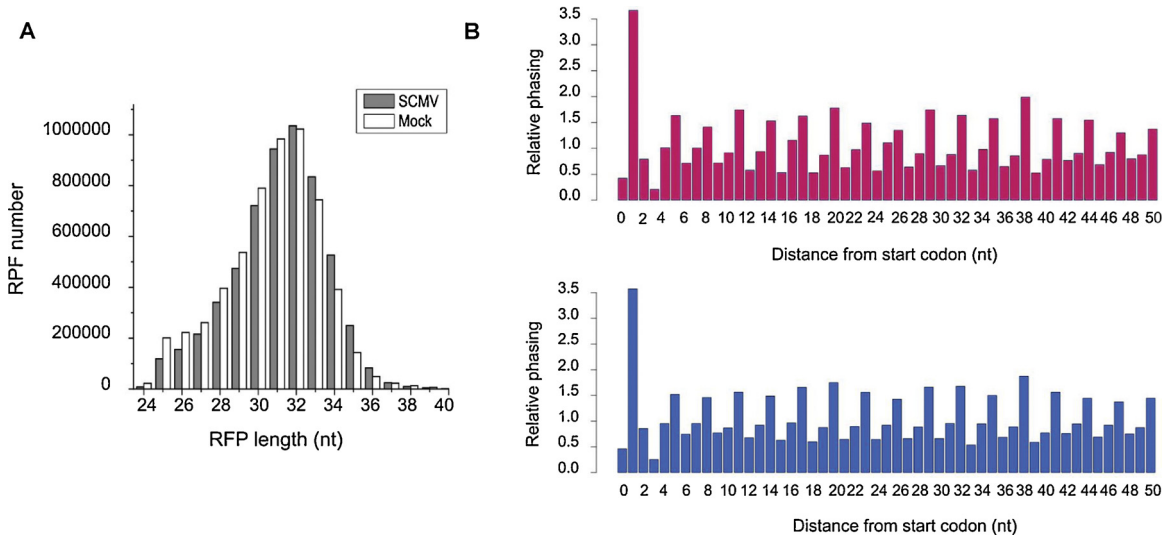

Fig. 2. Quality assessment of ribosome profiling data.
(A) Length distribution of ribosome-protected fragments (RPFs) in SCMV-infected (grey) and mock-inoculated (white) maize samples. (B) Three-nucleotide periodicity analysis in both SCMV-infected sample (top and purple) and mock-inoculated sample data (bottom and blue).

successfully implemented and were suitable for further studies.

3.3. Characteristics of the utilization of plant translational resources by SCMV

Plant viruses have evolved a compact structure for efficient amplification, which results in a complete dependence on the host translational systems (Gebauer and Hentze, 2004; Sanfaçon, 2015). However, the viral utilization of the plant translational resources has not been studied extensively. In SCMV-infected samples, only 1.43% to 2.45% total mapped reads were generated from SCMV genome, which suggests that this virus takes up only a small amount of host translational resources in the infection stage 3 (Table S2). Few SCMV mapped reads in mock samples were also found, which may result from a mismatch of short reads. Different from RNA sequencing, ribosome profiling library can indicate gene translational direction (Fig. 3A). Integrative Genomics Viewer (IGV) exhibition revealed that nearly all the RPFs of SCMV were produced from positive-stranded RNA of SCMV genome (Fig. 3A), confirming that only the genomic RNA encodes viral proteins. Among the mapped reads on the SCMV genome, 0.24% (228 reads) and 0.06% (54 reads) of the total SCMV-mapped reads were located in the 5′-UTR and 3′-UTR of viral genomic RNA, respectively. Correspondingly, 93,375 reads were mapped on the coding sequence of SCMV which accounted for 99.7% of the total SCMV reads. The proportions of encoding region mapped reads were higher than that in maize genes which was 97.5% (Lei et al., 2015), which was resulted from the difference of the genomic organization between SCMV and maize. We also found that the reads density was higher for either end of the genome than for the middle of the genome (Fig. 3A), indicating that initiation and termination are two rate-limiting steps in genome translation.

Our previous research showed that drought treatment would lead to translational repression on a genome-wide scale in maize and the polysome proportion significant decreased (Lei et al., 2015). To explore the effect of SCMV infection on maize translation, polysome content analyses were performed. Polysome-resuspended solutions obtained from both SCMV-infected and mock-inoculated samples were fractionated by centrifugation through sucrose gradients and each was conducted with four biological replicates (Fig. 4A). Contents of monosomes and polysomes were quantified by calculating corresponding peak areas (Fig. 4B). It revealed that the average polysome content (> 2 ribosomes) in SCMV-infected leaves was approximately 5% lower than in mock-inoculated leaves. However, Student *t*-test conducted showed that there was no significant difference ($p > 0.05$) between the overall polysome contents in SCMV- and mock-inoculated seedlings at 7 DPI. The result demonstrates that SCMV infection wouldn't significantly interrupt host translation system which is different from drought stress.

3.4. SCMV genome de novo assembly and SNP exploration

High-throughput sequencing is also a universal tool for genome assembly based on the information of overlapped fragments. Next, *de novo* SCMV genome assembly was performed with SCMV genome mapped reads based on RNA-seq and Ribo-seq data, respectively. As a result, six and nine contigs were constructed from RNA-seq data and Ribo-seq data after the whole genome alignment, respectively (Fig. 3B and Table S4). Contigs from RNA-seq data covered 88.24% of the genome with an average length of 1418 nt. The whole genome was well covered except of the viral coding sequence of HC-Pro and CI, which were partly covered with two gaps. Contigs of SCMV mapped reads from Ribo-seq data covered 75.8% of the genome with average 813 nt in length (Fig. 3B and Table S4). Segmented viral coding sequences of P3, 6K1, NIa-VPg, NIa-Pro and NIb were completely covered by the mapped reads, while HC-Pro, CI, 6K2, CP and 3′-UTR were partly covered. We also performed single nucleotide polymorphisms (SNPs) analysis by a comparison between assembled fragments and the reference genome. We identified 59 SNPs and 78 SNPs from RNA-seq data and Ribo-seq data, respectively. When relocating each SNP to viral protein-encoding region, we found that the first half of CI cistron (genome location: 3470–4651 nt) exhibited most variability with 59 SNPs of Ribo-seq data (Fig. 3B and Table S5). However, those SNPs located in the CI cistron gap of RNA-seq data. Combined with the distinct gaps we obtained from the IGV exhibiton result, it could be considered that CI as well as HC-Pro cistrons were among the most variable ones on the SCMV genome.

3.5. Global gene transcriptional and translational level changes in SCMV-infected maize leaves

The snapshot of translation provided by ribosome profiling should capture ribosomes more often on specific protein coding regions, thus indicating an importance of the proteins under certain circumstances. Cufflinks package (v2.2.1) was used to calculate the transcriptional and translational levels based on RNA-seq and Ribo-seq libraries, respectively. Fold change of gene expression (FPKM) was used to quantify and

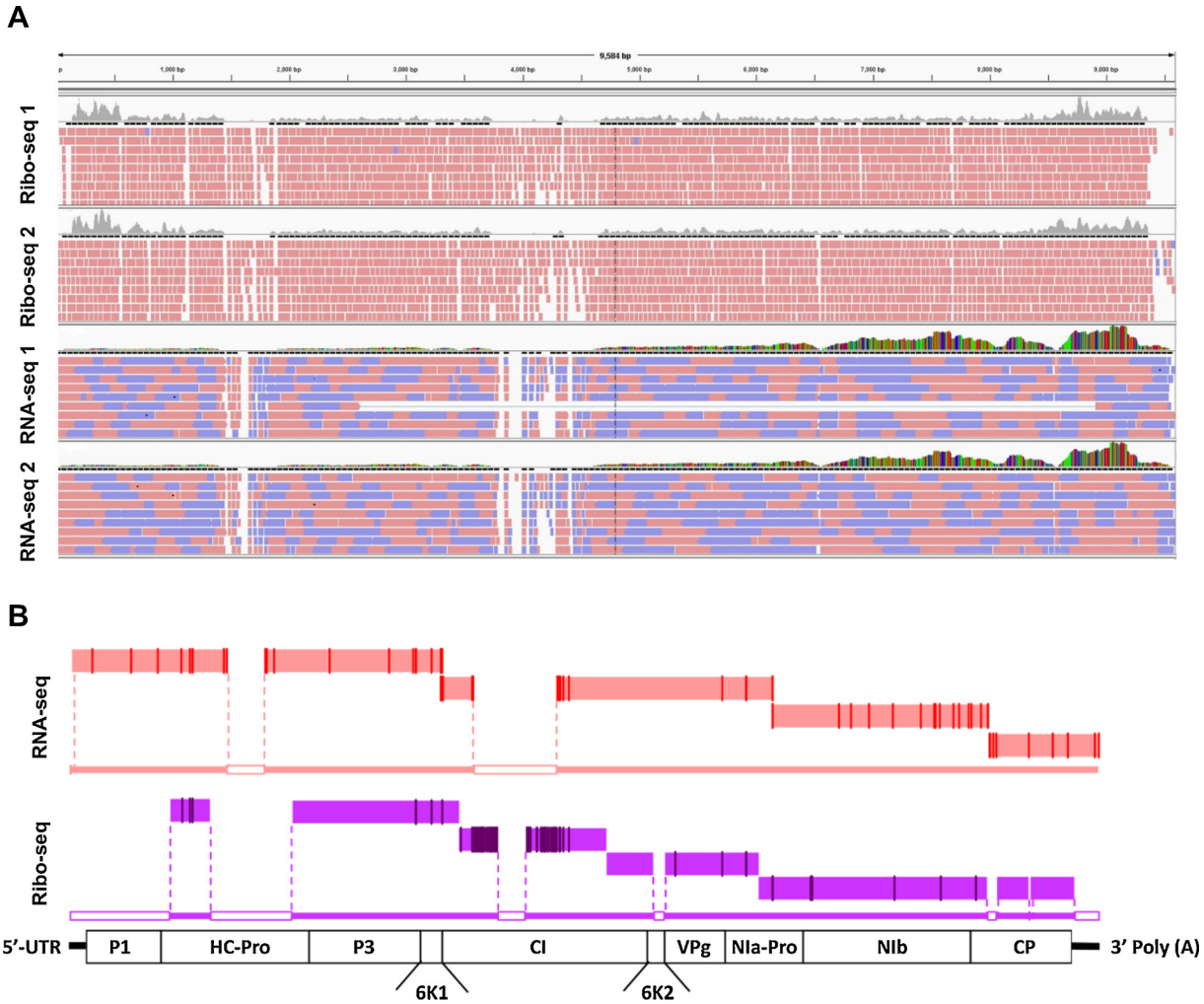

Fig. 3. *De novo* SCMV genomic fragments assembly.
IGV exhibition of the alignments on SCMV genome. Ribo-Seq and RNA-seq density of the SCMV genome was plotted on a linear scale marked as color bars. Positive-sense reads are shown in red while negative-sense reads are shown in blue on the top-right side below the horizontal axis. (B) Schematic representation of the assembled SCMV genomic fragments and SNPs. The assembled SCMV genomic fragments are drawing to scale in pink and purple from RNA-seq and Ribo-seq data, respectively. Vertical dark lines representing the SNP positions are embedded in the assembled fragments. The precise positions of the assembled fragments and SNPs are listed in Table S4 and Table S5, respectively.

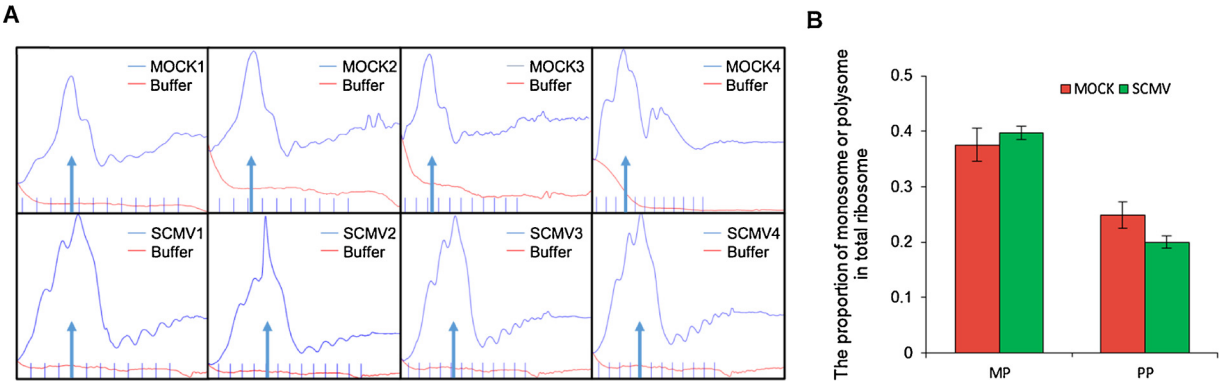

Fig. 4. Polysome level was not reduced upon SCMV infection.
(A) Analysis of polysome levels. Absorbance at 254 nm was electronically recorded with clarified ribosomes fractionated through sucrose density gradients. The baseline absorbance of a gradient loaded only with extraction buffer was shown as a red line. The position of monosomes is indicated with blue arrow. (B) Quantification of the change in polysome levels upon SCMV infection. MP and PP stand for the proportion of monosome and polysome, respectively. The red and green columns indicate MP (or PP) in mock-inoculated and SCMV-infected samples, respectively. The mean values and standard deviation were from four independent experiments. Values are means ± standard deviation (SD) (n = 4). Student's *t*-test was used for hypothesis testing (*P*-value > 0.05).

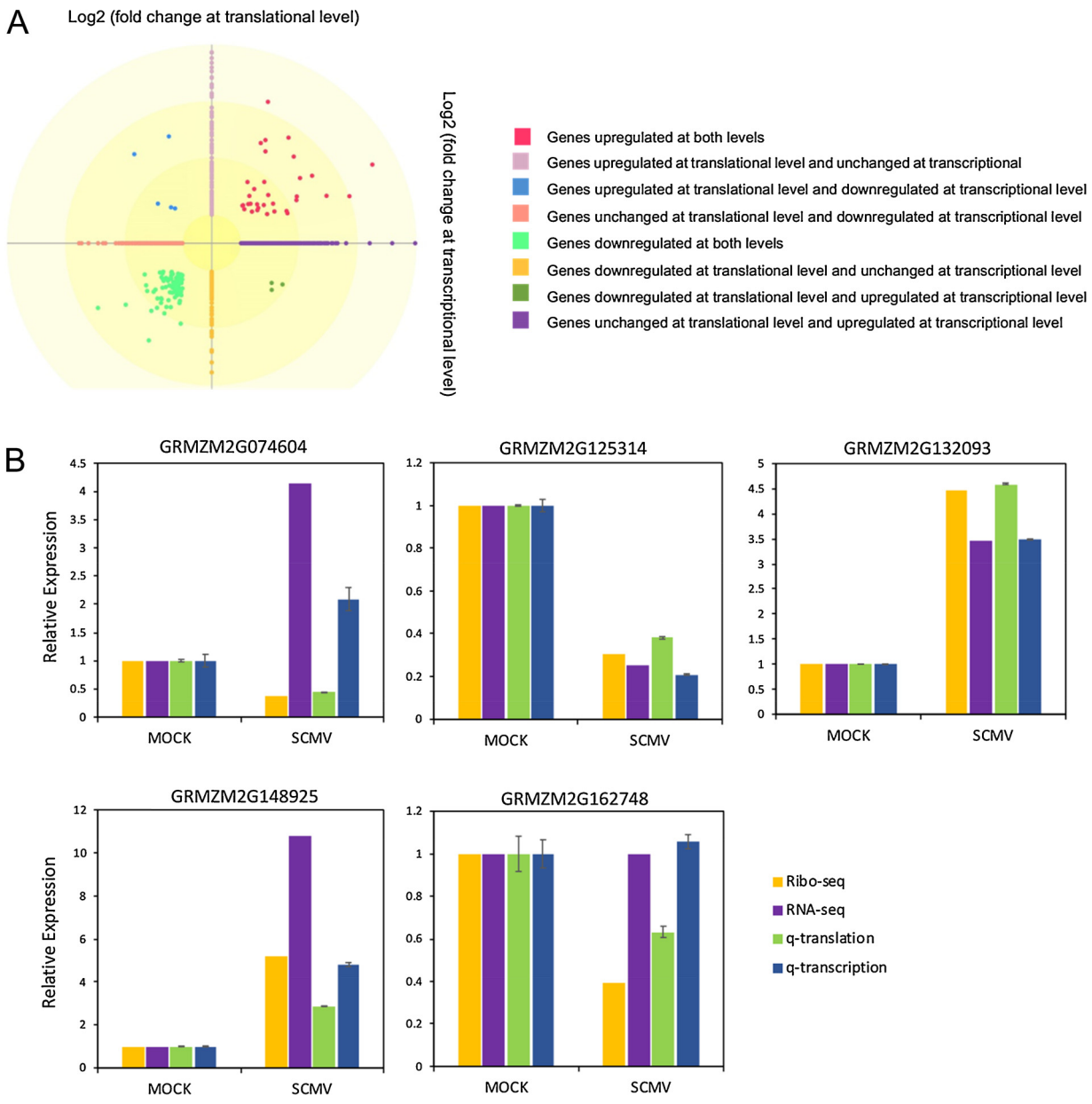

Fig. 5. SCMV infection induced transcriptional and translational responses.
(A) Fold changes of differentially expressed genes (DEGs) (fold change ≥ 2 and q-value ≤ 0.01) at transcriptional or translational levels upon SCMV-infection. Fold change of DEGs at transcriptional level form the x-coordinate and at translational level form the y-coordinate. (B) Validation of the Ribo-seq data by quantitative real-time PCR analysis of relevant maize genes. Expressions of 5 maize genes from Ribo-seq data (orange) and RNA-seq data (purple) are compared by real-time quantitative PCR data (green and blue, respectively). Templates for the qRT-PCR were cDNAs reverse-transcribed from the mRNA of polysome fractions and a total RNA extracted from leaf samples correspondingly, respectively. Three technical replicates were performed for each of three biological replicates. The height of each column represents the mean average of sample-specific $2^{-\Delta\Delta Ct}$ values, while associated error bars denote the standard error of the means. Functional annotation of these genes is listed in Table S6, Table S7, Table S8 and Table S9.

normalize gene expression levels. We identified 1012 up-regulated genes and 667 down-regulated genes with significant alteration at transcriptional level (Table S6 and S7). Meanwhile, 158 up-regulated genes and 326 down-regulated genes that were identified at translational level in the SCMV-infected maize seedlings, reflecting a higher number of modulated genes in the compatible host–virus interaction compared with the mock-inoculated samples (Table S8 and S9). There were 33 up-regulated genes and 93 down-regulated genes were shared between transcriptional and translational levels (Fig. 5A). Among the DEGs found in both levels, only 8 genes were reversely regulated (*i.e.* up-regulated in transcriptional and down-regulated in translational level, or *vice versa*) (Fig. 5A), reflecting that a discordant change at these two levels exists. The scatter diagram showed that the correlation between two levels was more significant for down-regulated genes than for the up-regulated genes, although in a medially concordant manner (Fig. 5A).

To validate the Ribo-Seq and RNA-seq results, five genes with different expression profiles were selected for further analysis by quantitative real-time RT-PCR (qRT-PCR). Templates for the qRT-PCR were cDNAs reverse-transcribed from the mRNA of polysome fractions correspondingly or total RNA, for Ribo-seq and RNA-seq results validation, respectively. As shown in Fig. 5B, the expression patterns of these genes determined by qRT-PCR were basically consistent with the results of Ribo-Seq and RNA-seq, confirming the accuracy of the data.

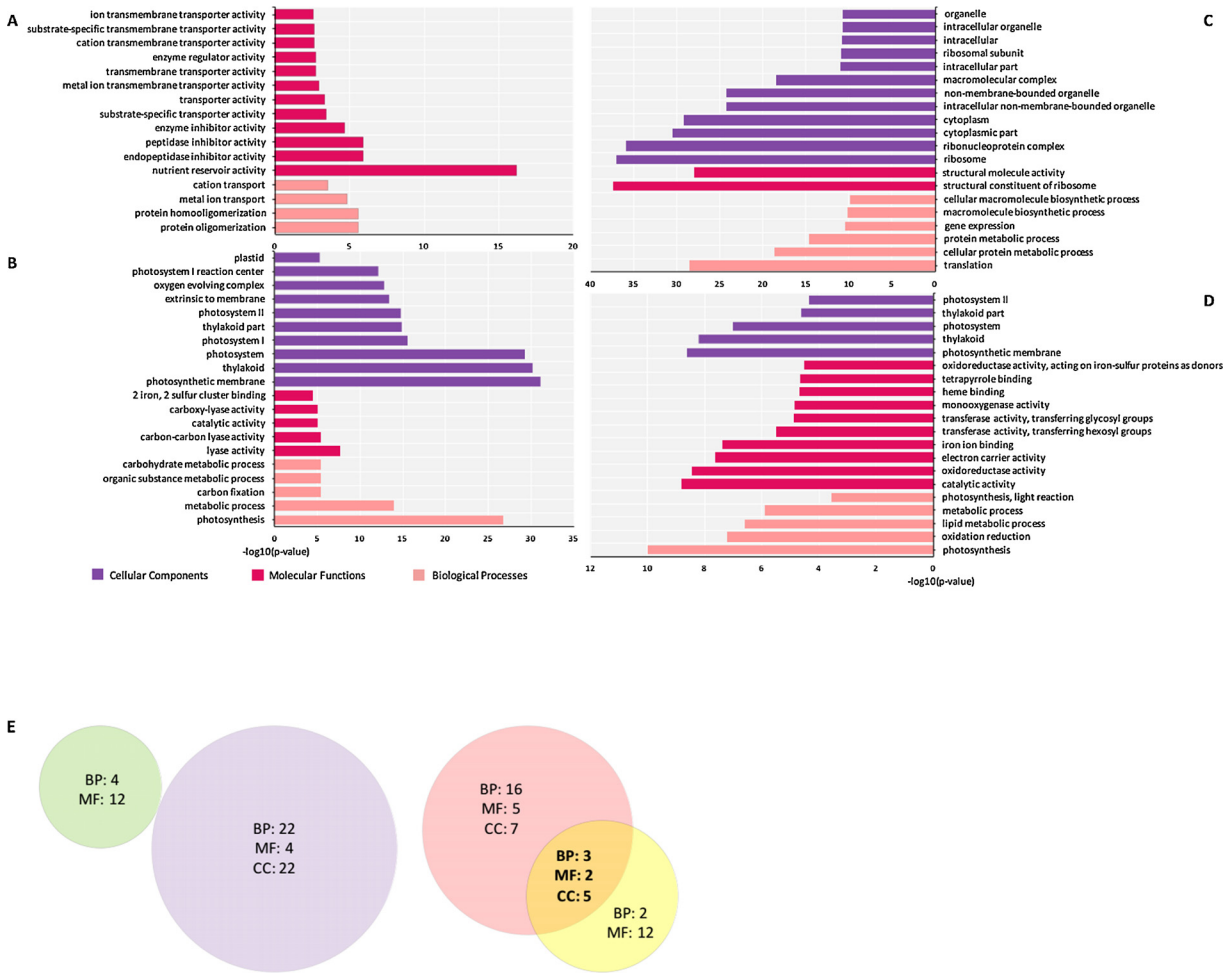

Fig. 6. GO annotation of differentially regulated genes post SCMV infection at translational and transcriptional levels.
GO analyses of up-regulated genes at **(A)** translational level and **(B)** transcriptional level, and down-regulated genes at **(C)** translational level and **(D)** transcriptional level, respectively. Purple, red and pink represent biological process, cellular component and molecular function, respectively. Significance of enrichment is indicated by a *p*-value of < 0.01. **(E)** Venn diagram showing GO terms overlap between translational (green and pink) and transcriptional level (purple and yellow) of up-regulated (left) and down-regulated genes (right), based upon the analytical data shown in Table S10. Down-regulated genes at both levels shared a total of ten enriched GO terms. They are photosynthesis, oxidation reduction and metabolic process of biological process category; lyase activity and catalytic activity of molecular finction category; photosynthetic membrane, thylakoid, photosystem, thylakoid part and photosystem II of cellular component category.

3.6. Gene ontology enrichment analysis

To examine the functional categories of these DEGs, GO enrichment analysis with AgriGO (Du et al., 2010) was performed. GO functional classifications allocated those DEGs at both transcriptional and translational levels of either up- or down-regulated into three main GO categories as biological processes, molecular functions and cellular components. The top 20 GO terms of each class is shown in Fig. 6. The complete GO classification data was listed in Table S10.

Nutrient reservoir activity (GO: 0045735) in molecular functions category was the most significantly enriched GO term among up-regulated genes at translational level, which suggested that the functions in the storage of nutritious substrates were incited by SCMV infection (Fig. 6A). Different kinds of transporter activities and enzymes inhibitor activities (GO: 0015075, GO: 0022857, GO: 0008324, GO: 0022891, GO: 0046873, GO: 0005215, GO: 0022892, GO: 0004857, GO: 0030414, GO: 0004866) were also induced (Fig. 6A and Table S10). As for the GO terms among the up-regulated genes at transcriptional level, most translational machinery related GO terms were significantly enriched (Fig. 6B and Table S10). Structural constituent of ribosomes (GO: 0003735) in the molecular function category was most significantly enriched, while ribosome (GO: 0005840) and translation (GO: 0006412) were the most enriched terms of the cellular components category and biological processes category, respectively (Fig. 6B and Table S10).

As the GO classifications indicated, photosynthesis related GO subterms were overwhelmingly enriched among the down-regulated genes at both levels (Fig. 6C and 6D). Besides, down-regulated genes at both levels shared a total of ten enriched GO terms, while up-regulated genes enriched terms at two levels shared no intersection (Fig. 6E). Moreover, the shared down-regulated genes between the two levels occupied the GO terms of photosynthesis- or metabolism-related, namely photosynthesis (GO: 0015979) and metabolic process (GO: 0008152) of the biological processes category, photosynthetic membrane (GO: 0034357), thylakoid (GO: 0009579) and photosystem (GO: 0009521) of the cellular components category.

4. Discussion

Since mRNA translation is subject to extensive regulation, it is difficult to systematically analyze SCMV genes expression as well as the translational responses of maize to SCMV infection through transcriptome analysis merely. Nevertheless, ribosome profiling, allowing only the actively translated segments of mRNAs recorded, can be the preferred technology to provide a snapshot *in vivo*. Our results revealed the translation profile of viral proteins and annotated maize genes

whose translational levels altered upon SCMV infection.

We analyzed the phenotypical responses of maize seedlings to SCMV-inoculation by recording the development of typical symptoms at 4, 6, 8, 10, 12 and 14 DPI on > 100 seedlings per treatment and dividing the infection process into several symptomatically distinct stages according to the distinct symptom phenotypes. At stage 3, positive-stranded RNA of the virus accumulated very rapidly and SCMV CP also accumulated to a certain titer. Since the genome expression of positive-stranded RNA viruses starts with translation rather than transcription (Tijms et al., 2001), we speculated that many translation-related components were recruited and began to function at this stage. In this scenario, we collected samples of this stage as the object for further ribosome profiling analysis to detect the translational responses to early SCMV infection.

In our analysis, about 2% RPFs were mapped to SCMV genome in total and the overall polysome content was not lowered, suggesting that stage 3 was an early stage for viruses to express their proteins as they occupied only a small amount of host translational resources. It is worth noting that RPFs from SCMV account for ~10.3% of the total RPFs in RNA-seq data (Table S2). Considering that ribosome profiling captures the translating mRNAs, the difference between 2% and 10.3% indicated that the proportion of negative-stranded RNA was relatively high. It could be inferred that the viral genome replication activity at this stage was strong.

Since single time-point detection showed restricted host regulatory events, several studies have employed ribosome profiling to study translational regulation kinetics after different intervals (Stern-Ginossar et al., 2012; Irigoyen et al., 2016). This strategy was exemplified in a previous study on HCMV. Upon the infection of HCMV, RPFs from this DNA virus accounted for 2.13% of the total RPFs from the human foreskin fibroblasts tissues at 4 h post infection (hpi). This percentage raised to 3.73% at 24 hpi, and up to 30.8% at 72 hpi (Stern-Ginossar et al., 2012). We propose that more translational apparatus as well as more regulatory mechanisms could be found in the SCMV-infected samples at late time-point.

Several studies were conducted previously on polysome contents changes among plants in response to abiotic and biotic stresses. Reduction in polysome content in response to abiotic stress seems to be common. Our previous study revealed that drought treatment leads the polysome proportion to be decreased by 16% in maize (Lei et al., 2015). Comparably, a study on rice showed that 17%–19% of the mRNA became dissociated with polysomes under the drought, salt or cold stress conditions (Park et al., 2012). Heat stress can also induce varying degrees of polysome content decrease in *Arabidopsis* (Matsuura et al., 2013). As to biotic stress, we found in this research that SCMV infection did not decrease the polysome content. Likewise, another previous study showed that overall levels of polysomes were not significantly altered either in barley upon the powdery mildew infection or in *Arabidopsis* upon the TuMV infection (Moeller et al., 2012). Despite the time-point selection differences, viral translational strategies should be considered.

Potyvirus-encoded proteins have been widely reported to interact with the host proteins to favor the viruses themselves, including HC-Pro, CP, CI, P1, P3 and P3-PIPO (Dawson, 1992; Shi et al., 2007; Cheng et al., 2008; Qiao et al., 2009). Previous research found that the interaction between soybean mosaic virus Pinellia isolate (SMV-P)-P1 and the mature Rieske Fe/S protein of the host by *in vitro* co-immunoprecipitation of the two proteins (Shi et al., 2007). Moreover, P1-Rieske Fe/S protein interactions are likely to be involved in symptom development. We also detected a repression of cytochrome b6-f complex Fe/S subunit in our work, suggesting that a possible inhibitory electron transport chain might be induced by P1 and the interaction. Ferredoxin-5 (FdV) participates in photosynthesis in three pathways including PSI, b6-f complex and redox control of the Calvin cycle. Our previous study demonstrated that FdV interacted with SCMV HC-Pro in maize protoplasts and was significantly down-regulated upon SCMV infection (Cheng et al., 2008). In our ribosome profiling library, we detected exactly the FdV (GRMZM2G122327) as the one mentioned above also with a negative regulation, which supported our previous study and suggested that the FdV played a role in the SCMV-maize interaction. Besides, several thioredoxin-ms (GRMZMG025954 and GRMZM181258) were also observed down-regulated as the interaction may also have an overall impact on the ferredoxin/thioredoxin system downstream.

As a pathogen, SCMV infection could stimulate various plant defense responses, but with a complex pattern (Whitham et al., 2006). As expected, many biotic stress-related and defense-related genes of the host were up-regulated post SCMV-infection, which strongly supports abundant previous studies with this technique. However, some of defense-related genes were detected to be down-regulated that differed from our expectation. It is known that reactive oxygen species (ROS) plays an important role in regulating biological processes response to biotic stresses and is also a collective term that includes both oxygen radicals like superoxide and other non-radicals like hydrogen peroxide (H_2O_2) (Del Rio, 2015; Xia et al., 2015). A previous study showed that expression of *ZmTrm2*, a gene encoding thioredoxin-m, was up-regulated at about 10 DPI by suppression subtractive hybridization under the infection of SCMV (Shi et al., 2011). However, we observed a down-regulated status of several thioredoxin-ms in our ribosome library of 7 DPI. Despite of some potential methodological differences and experimental biases, these results credibly indicated that the complex nature of host defense responses.

It should be noted that 8 genes are found reversely regulated (Fig. 5A). They are Aquaporin TIP3.1 (GRMZM2G037327), Uro-adherence factor A (Uraf A, GRMZM2G114182), Kinesin K39 (GRMZM2G118403), myo-inositol oxygenase (MIOX, GRMZM2G126900) and an unannotated gene (GRMZM2G470882), which are up-regulated at transcriptional level and down-regulated at translational level, while lysosomal β-glucosidase like (GRMZM2G017186), 4-coumarate coenzyme a ligase (4CL, GRMZM2G055320) and phenylalanine ammonia lyase (PAL, GRMZM2G074604) are down-regulated at transcriptional level and up-regulated at translational level, respectively. Among these, PAL has recently been found with an up-regulation in transcript abundance and a down-regulation at protein accumulation level also in the inoculated maize leaf sample upon SCMV infection but at 9 DPI in an iTRAQ data (Chen et al., 2017), which supports our result to some degree. Meanwhile, both PAL and 4CL are involved in the phenylpropanoid pathway (Li et al., 2015) and 4CL is also up-regulated at transcriptional level and down-regulated at translational level. It is speculated that post-transcriptional modification occurs to prevent their expression and find out the post-transcriptional regulators would help us to understand the role of phenylpropanoid pathway in SCMV infection.

GO analysis gives us an overview on enriched terms at both up- or down-regulated levels. However, Venn diagram showed us there was no overlap of up-regulated genes enriched GO terms between the transcriptional and translational responses (Fig. 6E), it seems that different categories of genes at the two levels were induced upon SCMV infection. We observed translational machinery related GO terms were enriched at transcriptional level while some biogenesis-related GO terms were enriched at translational level (Fig. 6B). Studies have been performed previously using P53 as an induction, regulation modes at two levels were also delineated. The results similarly showed a distinct mode of regulation between ribosome-biogenesis genes and ribosomal protein genes, which were mainly at the layer of transcription and translation, respectively (Loayza-puch et al., 2013). Coincidently, several ribosomal proteins and translation factors showed opposite regulation upon environmental stress in fission yeast (Lackner et al., 2012). We speculate that translational component genes which were up regulated in transcription (as displayed in Fig. 6B) may be accumulated temporarily, preparing for translation of the next infection stage. In accordance with our result, SCMV infection did not change the

translational level of maize. Further study should be conducted on the following infection stages to search for the regulation mode of differential gene expressions at both levels.

5. Conclusion

We first characterized SCMV infection process on maize systemically infected leaves and based on which, we selected stage 3 for our study since positive-stranded RNAs of the virus accumulated very rapidly and SCMV CP also accumulated to a certain titer at this stage. Utilization of plant translational resources by SCMV was studied since virus relies completely on the translational machinery of the host cell. We found that only the genomic positive-stranded RNA of SCMV was involved in translation, and SCMV only occupied a small amount of translational resources of host plant at stage 3. SNP analysis revealed that CI was shown as the most varied cistron. Global translational changes and GO enrichment analyses revealed that photosynthesis and metabolism was dramatically repressed. A global differential gene expression profile was obtained and significantly regulated candidates could be selected for further analysis. To our knowledge, this is the first application of ribosome profiling to a plant virus.

Author contributions

Z. F., L. L. and J. L. designed the study. T. X., L. L., J. S., X. W., J. C., M. X., S. S., B. Z., Z. X., N. J. and T. Z. performed the experiments. T. X., L. L. and Z. F. analyzed the data and wrote the manuscript.

Acknowledgements

This work was supported by grants from the Ministry of Agriculture (2016ZX08003-001), the Ministry of Science and Technology (No. 2016YFD0300710) and the Ministry of Education (the 111 Project B13006).

Appendix A. Supplementary data

Supplementary material related to this article can be found, in the online version, at doi:https://doi.org/10.1016/j.virusres.2018.10.013.

References

Charron, C., Nicolai, M., Gallois, J.L., Robaglia, C., Moury, B., Palloix, A., Caranta, C., 2008. Natural variation and functional analyses provide evidence for co-evolution between plant eIF4E and potyviral VPg. Plant J. 54, 56–68.
Chen, H., Cao, Y.Y., Li, Y.Q., Xia, Z.H., Xie, J.P., Carr, J.P., Wu, B.M., Fan, Z.F., Zhou, T., 2017. Identification of differentially regulated maize proteins conditioning *Sugarcane mosaic virus* systemic infection. New Phytol. 215, 1156–1172.
Cheng, Y.Q., Liu, Z.M., Xu, J., Zhou, T., Wang, M., Chen, Y.T., Li, H.F., Fan, Z.F., 2008. HC-Pro protein of sugarcane mosaic virus interacts specifically with maize ferredoxin-5 *in vitro* and *in planta*. J. Gen. Virol. 89, 2046–2054.
Chew, G.L., Pauli, A., Rinn, J.L., Regev, A., Schier, A.F., Valen, E., 2013. Ribosome profiling reveals resemblance between long non-coding RNAs and 5' leaders of coding RNAs. Development 140, 2828–2834.
Chung, B.Y., Miller, W.A., Atkins, J.F., Firth, A.E., 2008. An overlapping essential gene in the Potyviridae. Proc. Natl. Acad. Sci. U. S. A. 105, 5897–5902.
Dawson, W.O., 1992. Tobamovirus-plant interactions. Virology 186, 359–367.
Del Rio, L.A., 2015. ROS and RNS in plant physiology: an overview. J. Exp. Bot. 66, 2827–2837.
Du, Z., Zhou, X., Ling, Y., Zhang, Z., Su, Z., 2010. agriGO: a GO analysis toolkit for the agricultural community. Nucleic Acids Res. 38, W64–70.
Dunn, J.G., Foo, C.K., Belletier, N.G., Gavis, E.R., Weissman, J.S., 2013. Ribosome profiling reveals pervasive and regulated stop codon readthrough in *Drosophila melanogaster*. eLife 2, e01179.
Fan, Z.F., Chen, H.Y., Liang, X.M., Li, H.F., 2003. Complete sequence of the genomic RNA of the prevalent strain of a potyvirus infecting maize in China. Arch. Virol. 148, 773–782.
Gebauer, F., Hentze, M.W., 2004. Molecular mechanisms of translational control. Nature reviews. Mol. Cell Biol. 5, 827–835.
Gerashchenko, M.V., Lobanov, A.V., Gladyshev, V.N., 2012. Genome-wide ribosome profiling reveals complex translational regulation in response to oxidative stress. Proc. Natl. Acad. Sci. U. S. A. 109, 17394–17399.
Gibbs, A., Ohshima, K., 2010. Potyviruses and the digital revolution. Annu. Rev. Phytopathol. 48, 205–223.
Guttman, M., Russell, P., Ingolia, N.T., Weissman, J.S., Lander, E.S., 2013. Ribosome profiling provides evidence that large noncoding RNAs do not encode proteins. Cell 154, 240–251.
Hagiwara-Komoda, Y., Choi, S.H., Sato, M., Atsumi, G., Abe, J., Fukuda, J., Honjo, M.N., Nagano, A.J., Komoda, K., Nakahara, K.S., Uyeda, I., Naito, S., 2016. Truncated yet functional viral protein produced *via* RNA polymerase slippage implies underestimated coding capacity of RNA viruses. Sci. Rep. 6, 21411.
Herranz, M.C., Navarro, J.A., Sommen, E., Pallas, V., 2015. Comparative analysis among the small RNA populations of source, sink and conductive tissues in two different plant-virus pathosystems. BMC Genom. 16, 117.
Ingolia, N.T., Ghaemmaghami, S., Newman, J.R., Weissman, J.S., 2009. Genome-wide analysis *in vivo* of translation with nucleotide resolution using ribosome profiling. Science 324, 218–223.
Ingolia, N.T., Lareau, L.F., Weissman, J.S., 2011. Ribosome profiling of mouse embryonic stem cells reveals the complexity and dynamics of mammalian proteomes. Cell 147, 789–802.
Irigoyen, N., Firth, A.E., Jones, J.D., Chung, B.Y., Siddell, S.G., Brierley, I., 2016. High-resolution analysis of Coronavirus gene expression by RNA sequencing and ribosome profiling. PLoS Pathog. 12, e1005473.
Juntawong, P., Girke, T., Bazin, J., Bailey-Serres, J., 2014. Translational dynamics revealed by genome-wide profiling of ribosome footprints in Arabidopsis. Proc. Natl. Acad. Sci. U. S. A. 111, E203–212.
Kehoe, M.A., Coutts, B.A., Buirchell, B.J., Jones, R.A., 2014. Plant virology and next generation sequencing: experiences with a potyvirus. PLoS One 9 e104580-e104580.
Kneller, E.L., Rakotondrafara, A.M., Miller, W.A., 2006. Cap-independent translation of plant viral RNAs. Virus Res. 119, 63–75.
Kutnjak, D., Rupar, M., Gutierrez-Aguirre, I., Curk, T., Kreuze, J.F., Ravnikar, M., 2015. Deep sequencing of virus-derived small interfering RNAs and RNA from viral particles shows highly similar mutational landscapes of a plant virus population. J. Virol. 89, 4760–4769.
Lackner, D.H., Schmidt, M.W., Wu, S., Wolf, D.A., Bahler, J., 2012. Regulation of transcriptome, translation, and proteome in response to environmental stress in fission yeast. Genome Biol. 13, R25.
Langmead, B., Trapnell, C., Pop, M., Salzberg, S.L., 2009. Ultrafast and memory-efficient alignment of short DNA sequences to the human genome. Genome Biol. 10, R25.
Le, R.F.O., Candresse, T., Maule, A.J., Le, G.O., 1999. New advances in understanding the molecular biology of plant/potyvirus interactions. Mol. Plant Microbe Interact. 12, 367–376.
Lei, L., Shi, J., Chen, J., Zhang, M., Sun, S., Xie, S., Li, X., Zeng, B., Peng, L., Hauck, A., Zhao, H., Song, W., Fan, Z., Lai, J., 2015. Ribosome profiling reveals dynamic translational landscape in maize seedlings under drought stress. Plant J. 84, 1206–1218.
Léonard, S., Vie, C., Beauchemin, C., Daigneault, N., Fortin, M.G., Laliberté, J.F., 2004. Interaction of VPg-Pro of turnip mosaic virus with the translation initiation factor 4E and the poly(A)-binding protein in planta. J. Gen. Virol. 85, 1055–1063.
Li, Y., Kim, J.I., Pysh, L., Chapple, C., 2015. Four Isoforms of *Arabidopsis* 4-coumarate:CoA ligase have overlapping yet distinct roles in phenylpropanoid metabolism. Plant Physiol. 169, 2409–2421.
Liu, M.J., Wu, S.H., Wu, J.F., Lin, W.D., Wu, Y.C., Tsai, T.Y., Tsai, H.L., Wu, S.H., 2013. Translational landscape of photomorphogenic Arabidopsis. Plant Cell 25, 3699–3710.
Loayza-Puch, F., Drost, J., Rooijers, K., Lopes, R., Elkon, R., Agami, R., 2013. p53 induces transcriptional and translational programs to suppress cell proliferation and growth. Genome Biol. 14, R32.
Matsuura, H., Takenami, S., Kubo, Y., Ueda, K., Ueda, A., Yamaguchi, M., Hirata, K., Demura, T., Kanaya, S., Kato, K., 2013. A computational and experimental approach reveals that the 5'-proximal region of the 5'-UTR has a Cis-regulatory signature responsible for heat stress-regulated mRNA translation in Arabidopsis. Plant Cell Physiol. 54, 474–483.
Merits, A., Rajamaki, M.L., Lindholm, P., Runeberg-Roos, P., Kekarainen, T., Puustinen, P., Makelainen, K., Valkonen, J.P., Saarma, M., 2002. Proteolytic processing of potyviral proteins and polyprotein processing intermediates in insect and plant cells. J. Gen. Virol. 83, 1211–1221.
Michel, A.M., Choudhury, K.R., Firth, A.E., Ingolia, N.T., Atkins, J.F., Baranov, P.V., 2012. Observation of dually decoded regions of the human genome using ribosome profiling data. Genome Res. 22, 2219–2229.
Mingot, A., Valli, A., Rodamilans, B., León, D.S., Baulcombe, D.C., García, J.A., López-Moya, J.J., 2016. The P1N-PISPO *trans*-frame gene of sweet potato feathery mottle potyvirus is produced during virus infection and functions as an RNA silencing suppressor. J. Virol. 90, 3543–3557.
Moeller, J.R., Moscou, M.J., Bancroft, T., Skadsen, R.W., Wise, R.P., Whitham, S.A., 2012. Differential accumulation of host mRNAs on polyribosomes during obligate pathogen-plant interactions. Mol. Biosyst. 8, 2153–2165.
Nagano, A.J., Honjo, M.N., Mihara, M., Sato, M., Kudoh, H., 2015. Detection of plant viruses in natural environments by using RNA-Seq. Methods Mol. Biol. 1236, 89–98.
Nomoto, A., Katamura, N., Folini, F., Wimmer, E., 1977. The 5′ terminal structures of poliovirus RNA and poliovirus mRNA differ only in the genome-linked protein VPg. Proc. Natl. Acad. Sci. U. S. A. 77, 5345–5349.
Olspert, A., Chung, B.Y., Atkins, J.F., Carr, J.P., Firth, A.E., 2015. Transcriptional slippage in the positive-sense RNA virus family Potyviridae. EMBO Rep. 16, 995–1004.
Olspert, A., Carr, J.P., Firth, A.E., 2016. Mutational analysis of the *Potyviridae* transcriptional slippage site utilized for expression of the P3N-PIPO and P1N-PISPO proteins. Nucleic Acids Res. 44, 7618–7629.
Park, S.H., Chung, P.J., Juntawong, P., Bailey-Serres, J., Kim, Y.S., Jung, H., Bang, S.W., Kim, Y.K., Do Choi, Y., Kim, J.K., 2012. Posttranscriptional control of photosynthetic mRNA decay under stress conditions requires 3' and 5' untranslated regions and

correlates with differential polysome association in rice. Plant Physiol. 159, 1111–1124.
Qiao, Y., Li, H.F., Wong, S.M., Fan, Z.F., 2009. Plastocyanin transit peptide interacts with potato virus X coat protein, while silencing of plastocyanin reduces coat protein accumulation in chloroplasts and symptom severity in host plants. Mol. Plant Microbe Interact. 22, 1523–1534.
Riechmann, J.L., Lain, S., Garcia, J.A., 1992. Highlights and prospects of potyvirus molecular biology. J. Gen. Virol. 73 (Pt 1), 1–16.
Rodamilans, B., Valli, A., Mingot, A., León, D.S., Baulcombe, D., López-Moya, J.J., García, J.A., 2015. RNA polymerase slippage as a mechanism for the production of frameshift gene products in plant viruses of the *Potyviridae* family. J. Virol. 89, 6965–6967.
Sanfaçon, H., 2015. Plant translation factors and virus resistance. Viruses 7, 3392–3419.
Shalgi, R., Hurt, J.A., Krykbaeva, I., Taipale, M., Lindquist, S., Burge, C.B., 2013. Widespread regulation of translation by elongation pausing in heat shock. Mol. Cell 49, 439–452.
Shi, Y., Chen, J., Hong, X., Chen, J., Adams, M.J., 2007. A potyvirus P1 protein interacts with the Rieske Fe/S protein of its host. Mol. Plant Pathol. 8, 785–790.
Shi, Y., Qin, Y.H., Cao, Y.Y., Sun, H., Zhou, T., Hong, Y.G., Fan, Z.F., 2011. Influence of an m-type thioredoxin in maize on potyviral infection. Eur. J. Plant Pathol. 131, 317–326.
Shukla, D.D., Tosic, M., Jilka, J., Ford, R.E., Toler, R.W., Langham, M.A.C., 1989. Taxonomy of potyviruses infecting maize, sorghum, and sugarcane in Australia and the United States as determined by reactivities of polyclonal antibodies directed towards virus-specific N-termini of coat proteins. Phytopathology 169, 223–229.
Stern-Ginossar, N., Weisburd, B., Michalski, A., Le, V.T., Hein, M.Y., Huang, S.X., Ma, M., Shen, B., Qian, S.B., Hengel, H., Mann, M., Ingolia, N.T., Weissman, J.S., 2012. Decoding human cytomegalovirus. Science 338, 1088–1093.
Tijms, M.A., Vandinten, L.C., Gorbalenya, A.E., Snijder, E.J., 2001. A zinc finger-containing papain-like protease couples subgenomic mRNA synthesis to genome translation in a positive-stranded RNA virus. Proc. Natl. Acad. Sci. U. S. A. 98, 1889–1894.
Trapnell, C., Pachter, L., Salzberg, S.L., 2009. TopHat: discovering splice junctions with RNA-Seq. Bioinformatics 25, 1105–1111.
Untiveros, M., Olspert, A., Artola, K., Firth, A.E., Kreuze, J.F., Valkonen, J.P., 2016. A novel sweet potato potyvirus open reading frame (ORF) is expressed via polymerase slippage and suppresses RNA silencing. Mol. Plant Pathol. 17, 1111–1123.
Urcuqui-Inchima, S., Haenni, A.L., Bernardi, F., 2001. Potyvirus proteins: a wealth of functions. Virus Res. 74, 157–175.
Whitham, S.A., Yang, C., Goodin, M.M., 2006. Global impact: elucidating plant responses to viral infection. Mol. Plant Microbe Interact. 19, 1207–1215.
Wylie, S.J., Luo, H., Li, H., Jones, M.G., 2012. Multiple polyadenylated RNA viruses detected in pooled cultivated and wild plant samples. Arch. Virol. 157, 271–284.
Xia, X.J., Zhou, Y.H., Shi, K., Zhou, J., Foyer, C.H., Yu, J.Q., 2015. Interplay between reactive oxygen species and hormones in the control of plant development and stress tolerance. J. Exp. Bot. 66, 2839–2856.
Xia, Z., Peng, J., Li, Y., Chen, L., Li, S., Zhou, T., Fan, Z., 2014. Characterization of small interfering RNAs derived from sugarcane mosaic virus in infected maize plants by deep sequencing. PLoS One 9, e97013.